Communications Research Centre

AN IMPROVED CHA ALGORITHM FOR TRACKING LOW-ANGLE TARGETS (U)

by

B.J. Rook and J. Litva

This document was prepared for and is the property of the Department of National Defence.

This work was sponsored by the Department of National Defence, Research and Development Branch under Project No. 33C70.

DEPARTMENT OF COMMUNICATIONS
MINISTERE DES COMMUNICATIONS

CRC REPORT NO. 1356

CANADA

OTTAWA, APRIL 1982

TABLE OF CONTENTS

COMMUNICATIONS RESEARCH CENTRE

DEPARTMENT OF COMMUNICATIONS
CANADA

AN IMPROVED CHA ALGORITHM FOR TRACKING LOW-ANGLE TARGETS(U)

by

B.J. Rook and J. Litva

(Radar and Communications Technology Branch)

CRC REPORT NO. 1358

April 1982

OTTAWA

This work was sponsored by the Department of National Defence, Research and Development Branch under Project No. 33C70.

AN IMPROVED CHA ALGORITHM FOR TRACKING LOW-ANGLE TARGETS(U)

by

B.J. Rook and J. Litva

ABSTRACT

An improved Correlation Height Analysis (CHA)[1] algorithm is described and further supporting evidence for its effectiveness is provided. The underlying principles are the same as the original CHA algorithm, namely; (a) modelling the behavior of tracking radars in the low-angle region; (b) comparing results of the model with measured data in a correlation process; and (c) selecting the true track from the family of tracks provided by the correlator. The improvements to be discussed are concerned mainly with increasing the efficiency and robustness of the algorithm. The most significant is the procedure for effecting item (c). In addition, a description is given of the software implementation of the algorithm together with the sampled-aperture radar facility used to record data for testing the algorithm. CHA low-angle tracking is demonstrated using experimental data recorded with this facility.(U)

1. INTRODUCTION

In recent years, a considerable amount of research has been devoted to finding a solution to the problem of tracking targets in the low-angle region, in particular, when these targets are tracked over the surface of the sea. In this region, the performance of conventional tracking radars is seriously degraded owing to the reflection of radar signals by the surface of the water. The main thrust of the research in this area has been directed towards finding methods for eliminating or at least reducing the degrading effect of the reflected or indirect signal so as to improve the tracking accuracy of the radar.

Litva[1] has described a technique whereby advantage is taken of the information due to multipath contained in the composite signal detected by

the radar. This technique, which is known as the Correlation Height Analysis (CHA) technique, uses a model to simulate the multipath propagation in this region. The height of the target is derived by cross-correlating theoretical data obtained from the model with measured data. It should be noted that the technique identifies a family of target tracks all of which are initially equally likely.

In this report, the formulation of an improved CHA algorithm is described. In addition, recent results are presented to demonstrate the capability of this algorithm with experimental data.

2. ASSUMPTIONS

In the following mathematical development leading to the derivation of the correlation function, simple ray theory is used to describe the interference between two waves following a direct and an indirect path. In this description, it is assumed that there is only one reflecting surface and that this surface is perpendicular to the vertical at the point of reflection. If, in practice, it is found that the presence of surface tilts so degrades the performance of the algorithm, it is further assumed that these effects can be made to be negligible by assorted techniques such as, range averaging of the radar signal and modelling the tilts using data from sensors placed aboard the ship.

3. PLANE-EARTH GEOMETRY

In the development of formulae to describe accurately the signal detected by the radar in the low-angle region we first consider the plane-earth geometry which is shown in Figure 1. Here, we have a radar antenna at height z_1 above a horizontal plane and a target at height z_2 above the same plane. The composite signal detected by the radar, assuming the antenna to be isotropic, is the sum of E_d the direct signal due to a plane-wave along the direct path and E_i the indirect signal due to a plane-wave reflected from the surface of the earth.

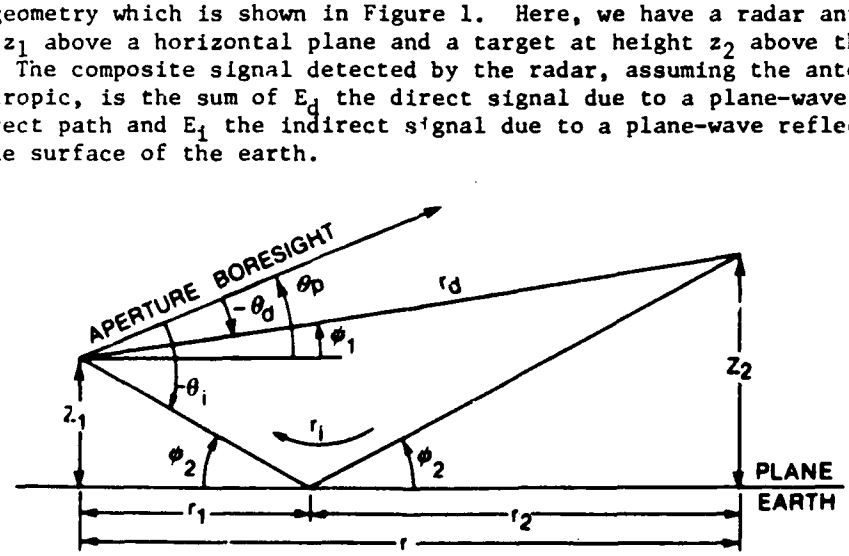

Figure 1. Low-angle Geometry (Plane Earth)

For the moment, we shall asume that the presence of the plane-earth can be represented by the plane-wave reflection coefficient Γ which is a function of the grazing angle ψ_2, and is, in general, a complex quantity represented by

$$\Gamma \equiv \rho\, e^{-j\phi}, \qquad 0 \leq \rho \leq 1. \tag{1}$$

The quantity ρ gives the reduction in the amplitude of the signal on reflection and ϕ gives its phase retardation. In the following sub-section, the composite signal observed at z_1 due to the presence of the direct and indirect signals is formulated and discussed.

3.1 FORMULATION OF THE COMPOSITE SIGNAL OBSERVED AT z_1

In formulating the composite signal at z_1, let the direct signal E_d be given by

$$E_d = E_o\, e^{j(\omega t - kr_d)} \tag{2}$$

where

E_o = the amplitude

ω = the angular frequency

r_d = the length of the direct path, and

$k = \frac{2\pi}{\lambda}$ is the wave number, λ being the free-space wavelength.

Similarly, let the indirect signal E_i be given as

$$E_i = E_o\, \rho\, e^{j(\omega t - kr_i - \phi)} \tag{3}$$

where r_i is the length of the indirect path. The composite signal observed at z_1 is simply the sum of E_d and E_i, thus

$$E_d + E_i = E_o\, e^{j(\omega t - kr_d)} \left[1 + \rho\, e^{-j\{\phi + k(r_i - r_d)\}}\right] . \tag{4}$$

Equation (4) defines an interference pattern in space whose shape is given by the quantity inside the square brackets. The factor outside the brackets gives the signal that would be observed if only the direct ray were present. This interference pattern is of considerable importance in that its detailed shape depends upon the location of the target. Insofar as modelling the multipath propagation in the low-angle region (interference region) is concerned, our only interest is in the amplitude and phase of the indirect signal relative to the direct signal, consequently, the factor outside the

square brackets may be discarded. Therefore, eqn. (4) may be rewritten giving

$$E = 1 + \rho\, e^{-j\{\phi+k(r_i-r_d)\}} \quad . \tag{5}$$

Thus, eqn. (5) describes, in complex form, the interference pattern at z_1 due to the superposition of two signals which have related amplitude and phase characteristics.

From the geometry of Figure 1, the lengths of the direct and indirect paths may be determined to be

$$r_d = [r^2 + (z_2-z_1)^2]^{1/2} \tag{6}$$

and

$$r_i = [r^2 + (z_1+z_2)^2]^{1/2} \quad , \tag{7}$$

therefore, the path-length difference $\Delta r = r_i - r_d$ may be determined by expanding each path length by the binomial theorem and subtracting, to wit

$$\Delta r = \frac{2z_1z_2}{r}\left[1 - \frac{z_1^2+z_2^2}{2r^2} + \ldots\right] \quad . \tag{8}$$

This expression is unwieldly, but fortunately in the low-angle region, that is, where ψ_1 and ψ_2 are small, the expression may be simplified to the more usual form of

$$\Delta r \cong \frac{2z_1z_2}{r} \quad , \tag{9}$$

with $r = r_d$, the slant or measured radar range to the target. Therefore, we may rewrite eqn. (5), giving

$$E = 1 + \rho\, e^{-j(\phi+k\Delta r)} \tag{10}$$

Thus, eqns. (9) and (10) map out the phase and amplitude of an interference pattern observed at z_1 as a function of r and z_2. Alternatively, if r and z_2 are considered to be constant, eqns. (9) and (10) map out the phase and amplitude of an interference pattern as a function of z_1. From this it follows that if a number of elements were vertically disposed above the horizontal plane at the receiving end, we may, at least conceptually, sample simultaneously the phase and amplitude at the element positions for given values of r and z_2. Thus, we have introduced the concept of the sampled aperture, whereby we sample the composite signal at discrete intervals on a finite straight line in space at some instant of time where, at this instant, r and z_2 are considered to be constant. The concept of the sampled aperture and its application to solving the low-angle tracking problem is of considerable importance, and will be discussed in much greater detail later in this report.

Suffice it to say that in order to describe the relative phase and amplitude distribution across this aperture, eqn. (10) must be evaluated. However, this equation cannot be evaluated until a complete knowledge of the behavior of ρ and ϕ is known. In addition, since a sampled aperture is being considered, the distribution of phase across this aperture for varying angles-of-arrival of the direct and indirect signals must also be known.

3.2 DETERMINATION OF THE ANGLES-OF-ARRIVAL OF THE DIRECT AND INDIRECT SIGNALS

To fully describe the resultant phase and amplitude distribution across the sampled aperture for a given r and z_2, we must be able to calculate the angles-of-arrival of the direct and indirect signals relative to the boresight of the aperture. After carrying out these calculations, we then find that we are able to derive the quantities ρ and ϕ which, in turn, leads to an evaluation of eqn. (10).

In deriving formulae to determine the angles-of-arrival of the direct signal θ_d and the indirect signal θ_i relative to the boresight of the aperture it is necessary to establish a convention for signs for the angles shown in Figure 1. The angles ψ_1, ψ_2 and θ_p (the pointing angle) are measured positive upwards from the horizontal line, whereas the angles θ_d and θ_i are measured positive upwards from the aperture boresight. In the construction of Figure 1, both θ_d and θ_i are shown to be numerically negative. It follows that

$$\tan\psi_1 = \frac{z_2-z_1}{r} \tag{11}$$

and

$$\tan\psi_2 = \frac{z_1+z_2}{r} \quad . \tag{12}$$

In the low-angle region, where ψ_1 and ψ_2 are small, eqn. (11) and eqn. (12) reduce to

$$\psi_1 \cong \frac{z_2-z_1}{r} \tag{13}$$

and

$$\psi_2 \cong \frac{z_1+z_2}{r} \quad , \tag{14}$$

whereupon the angles-of-arrival of the direct signal θ_d and the indirect signal θ_i relative to the aperture boresight, may be given as

$$\theta_d = \psi_1-\theta_p \tag{15}$$

and

$$\theta_i = -(\psi_2+\theta_p) \quad . \tag{16}$$

From the preceding we note that in the process of deriving θ_d and θ_i we have also obtained the grazing angle ψ_2.

3.3 DETERMINATION OF THE PLANE-EARTH REFLECTION COEFFICIENT

The plane-earth reflection coefficient, which is in general a complex quantity, is given by eqn. (1). The evaluation of this equation is based primarily on a knowledge of the grazing angle ψ_2 and the electrical properties of the reflecting surface. For a smooth plane surface, the complex reflection coefficient may be given for either vertically or horizontally polarized waves[3] as

$$\Gamma_V \equiv \rho_V e^{-j\phi_V} = \frac{\varepsilon_c \sin(\psi_2) - \sqrt{\varepsilon_c - \cos^2(\psi_2)}}{\varepsilon_c \sin(\psi_2) + \sqrt{\varepsilon_c - \cos^2(\psi_2)}} \tag{17}$$

and

$$\Gamma_H \equiv \rho_H e^{-j\phi_H} = \frac{\sin(\psi_2) - \sqrt{\varepsilon_c - \cos^2(\psi_2)}}{\sin(\psi_2) + \sqrt{\varepsilon_c - \cos^2(\psi_2)}} \tag{18}$$

where the subscripts V and H denote vertical and horizontal polarization respectively.

The term ε_c in eqns. (17)-(18) is known as the complex dielectric constant of the surface and is given as

$$\varepsilon_c = \frac{\varepsilon}{\varepsilon_o} - j\frac{\sigma}{\omega\varepsilon_o} \tag{19}$$

where $\varepsilon/\varepsilon_o$ = the ratio of the dielectric constant of the surface to that of free space

σ = the conductivity of the surface in mho/m

$\varepsilon_o = 8.84 \times 10^{-12}$ Farads/m is the dielectric constant of free space.

Alternatively, eqn. (19) may be expressed in terms of the wavelength λ as

$$\varepsilon_c = \frac{\varepsilon}{\varepsilon_o} - j\,60\lambda\sigma \tag{19a}$$

provided λ is expressed in metres.

The values of $\varepsilon/\varepsilon_o$ and σ to be used in eqn. (19) and (19a) are determined by the characteristics of the surface that is under consideration. Values for $\varepsilon/\varepsilon_o$ and σ over sea-water and fresh-water surfaces are given in Table 1. The electrical properties of these two surfaces were chosen since they represent the extremes of the range of water surfaces that are likely to be encountered in practice.

TABLE 1

Electrical Properties of Water

Surface	σ mho/m	ϵ/ϵ_o
Sea-water	4.3	80
Fresh-water	10^{-2}	80

If we note that in the low-angle region ψ_2 is small and that for either sea-water or fresh-water $|\epsilon_c| >> 1$, then eqn. (17) and (18) may be simplified to

$$\Gamma_V = \rho_V e^{-j\phi_V} \cong \frac{\psi_2 \sqrt{\epsilon_c} - 1}{\psi_2 \sqrt{\epsilon_c} + 1} \tag{20}$$

and

$$\Gamma_H = \rho_H e^{-j\phi_H} \cong \frac{\psi_2 - \sqrt{\epsilon_c}}{\psi_2 + \sqrt{\epsilon_c}} \quad . \tag{21}$$

Figure 2 shows plots of the magnitude of the reflection coefficient ρ against grazing angle ψ_2 for vertically and horizontally polarized waves over a perfectly smooth sea-surface. Figure 3 gives plots of the phase of the reflection coefficient for vertically and horizontally polarized waves. These results were calculated with eqns. (17)-(18) using a wavelength $\lambda = 0.032$m (X-band).

4. CURVED-EARTH GEOMETRY

As the value of r increases, the foregoing mathematical expressions become increasingly inaccurate because of the curvature of the earth. In order to correct for this curvature, we must now consider the curved-earth geometry given in Figure 4. Insofar as the low-angle region (interference region) is concerned, the diagram of Figure 4 is grossly exagerated, however, it has been presented in this manner in order to clearly define the quantities of interest.

Since we are dealing with a curved-earth rather than a plane-earth geometry a new quantity, namely, the divergence factor must be introduced. The divergence factor, denoted D, gives a measure of the defocussing that occurs when an electromegnetic wave is reflected from a curved surface. How-

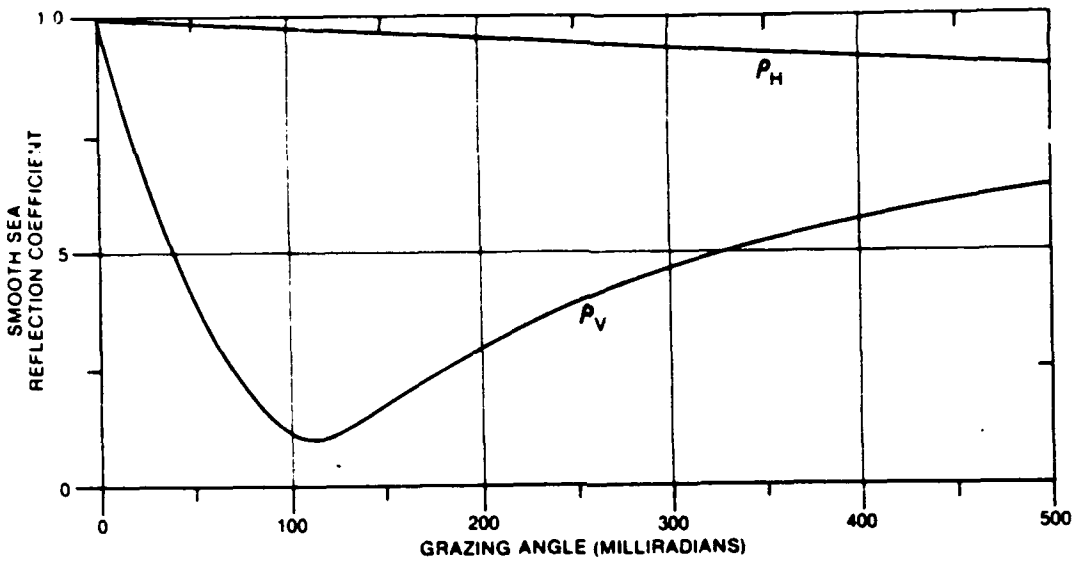

Figure 2. Vertical and Horizontal Reflection Coefficient Magnitudes

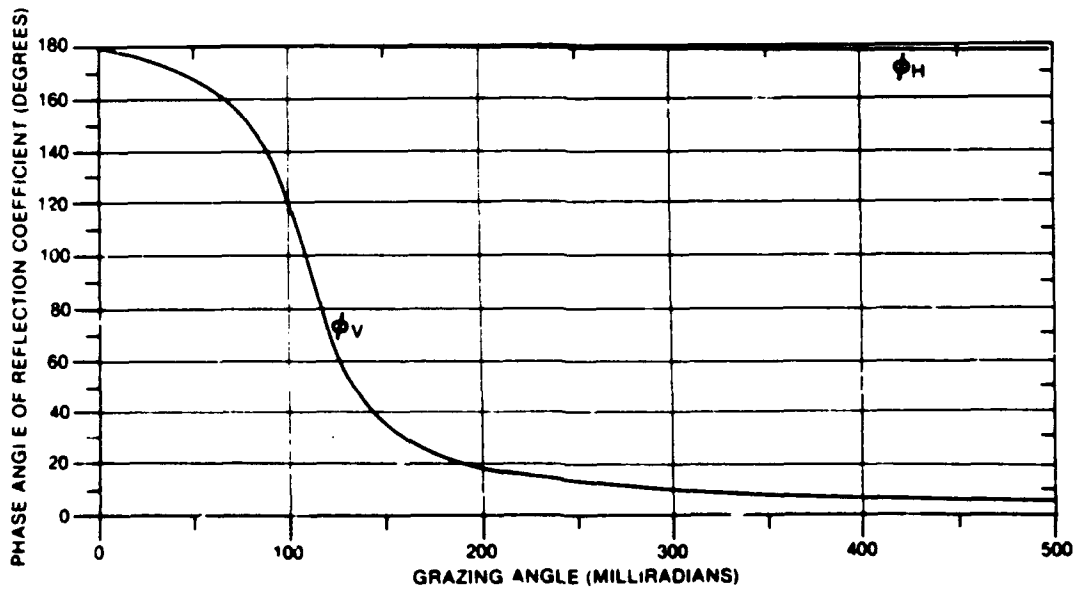

Figure 3. Vertical and Horizontal Reflection Coefficient Phases

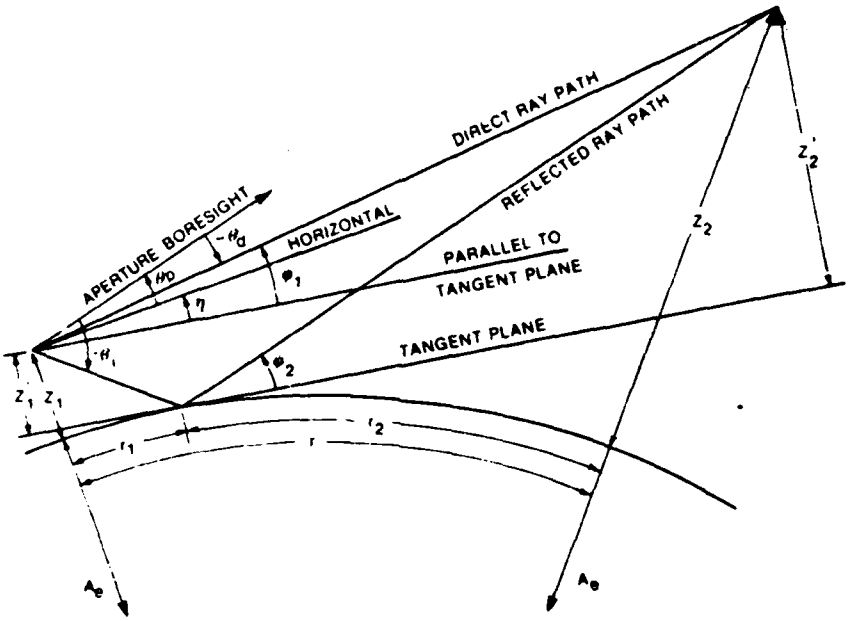

Figure 4. Low-angle Geometry (Curved Earth)

ever, before this and other related quantities may be determined, the distance from either terminal point to the reflecting point must first be calculated.

4.1 DERIVATION OF THE POINT OF REFLECTION ON A CURVED SURFACE

When dealing with a plane-earth geometry we found that the parameters that had the greatest impact when deriving interference patterns (see eqn. (10)) were the path-length difference Δr and the grazing angle ψ_2. This is also true for a curved-earth geometry, but first we must determine the position of the reflecting point, or how r is broken into the length r_1 and r_2. Once r_1 and r_2 have been determined, corrected values for Δr and ψ_2 may be calculated.

If we are given the values of z_1, z_2 and r, it is possible to find r_1 by solving the cubic equation[4]

$$f(r) = 2r_1^3 - 3r_1^2 r + [r^2 - 2A_e(z_1+z_2)]r_1 + 2A_e z_1 r = 0, \qquad (22)$$

where A_e is the effective earth's radius, normally taken to be 8.5×10^6 m.

This cubic equation has the formal solution:

$$r_1 = \frac{r}{2} + p \cos\left(\frac{\Phi+\pi}{3}\right) \quad ,$$

where

$$p = \frac{2}{\sqrt{3}} \sqrt{A_e(z_1+z_2) + \left(\frac{r}{2}\right)^2} \tag{23}$$

and

$$\Phi = \cos^{-1}\left[\frac{2A_e(z_2-z_1)r}{p^3}\right].$$

Unfortunately, the formal solution to this equation is not very practical for implementation on a digital computer, particularly when one considers that there is an inverse cosine to be evaluated. A more practical method for its solution is described in the following sub-section.

4.2 NEWTON'S METHOD FOR SOLVING THE CUBIC EQUATION

An efficient method for solving the cubic equation with a digital computer is by using Newton's[5] method. When written in its recursive form, Newton's method take: the form

$$(r_1)_{n+1} = (r_1)_n - \frac{f[(r_1)_n]}{f'[(r_1)_n]} \quad . \tag{24}$$

The parentheses surrounding r_1 are to distinguish the subscript of r from the index n of the recursion formula.

Initially, $(r_1)_{n=1}$ is assigned a value which is near the desired root of the cubic equation. This value is determined by noting from the plane-earth geometry of Figure 1 that

$$(r_1)_{n=1} = \frac{rz_1}{z_1+z_2} \quad . \tag{25}$$

Equation (24) is then computed in an iterative manner until $|(r_1)_n-(r_1)_{n+1}| \leq 1.0m$. In practice, three iterations of eqn. (24) are required for this inequality to be satisfied.

4.3 DETERMINATION OF THE PATH-LENGTH DIFFERENCE

Once the position of the reflecting point has been determined, we may then compute all other quantities of interest relative to the plane which is tangent to the surface of the earth ar r_1.

To begin, we calculate new values of z_1 and z_2, namely z_1' and z_2'. Referring to Figure 4, it is convenient to define parameters ℓ_1 and ℓ_2 which give distances from the tangent plane to the earth's surface. For small angles they are

$$\ell_1 \cong z_1 - z_1' \tag{26}$$

and

$$\ell_2 \cong z_2 - z_2' \quad . \tag{27}$$

In the low-angle region where ψ_1 and ψ_2 are small, the distance along the tangent plane from the respective terminal points to the reflection point may be taken to be r_1 and r_2. In a straight forward manner[6] it can be shown that

$$\ell_{1,2} \cong \frac{r_{1,2}^2}{2A_e} \tag{28}$$

from which the new heights z_1' and z_2' may be determined thus,

$$z_1' \cong z_1 - \frac{r_1^2}{2A_e} \tag{29}$$

and

$$z_2' \cong z_2 - \frac{r_2^2}{2A_e} \quad . \tag{30}$$

Be referring to Figures (1) and (4) and using eqn. (9), the corrected path-length difference can be written as

$$\Delta r \cong \frac{2z_1'z_2'}{r} \quad . \tag{31}$$

4.4 DETERMINATION OF θ_d and θ_i

The calculation of the angles-of-arrival for the direct and indirect signals, θ_d and θ_i respectively, are carried out in a manner similar to that for the plane-earth case, with the exception of now having to consider η, which is the angle between the horizontal plane and a plane parallel to the tangent plane.

It follows from an inspection of Figure 4 that

$$\eta = \frac{r_1}{A_e} \quad . \tag{32}$$

Furthermore,

$$\psi_1 \cong \frac{z_2'-z_1'}{r} \tag{33}$$

and

$$\psi_2 \cong \frac{z_1'+z_2'}{r}, \tag{34}$$

whereupon the angles-of-arrival of the direct and the indirect signals relative to the aperture boresight are

$$\theta_d = \psi_1 - \theta_p - \eta \tag{35}$$

and

$$\theta_i = -(\psi_2 + \theta_p + \eta). \tag{36}$$

4.5 THE DIVERGENCE FACTOR

When a bundle of parallel rays is incident on the convex side of a curved surface, the rays diverge after reflection because each has a slightly different angle of incidence. Because of this divergence, the reflected signal is defocussed and the power density is reduced. The divergence factor can be derived solely from geometrical considerations[7] and is given here in a form which incorporates the usual approximations which are applicable in the low-angle region, namely

$$D \cong \frac{1}{\sqrt{1 + \frac{2r_1 r_2}{A_e r \psi_2}}}. \tag{37}$$

5. SURFACE ROUGHNESS FACTOR

The discussion thus far has been based on the assumption that the surface was smooth in the neighborhood of the specular reflecting point. We now consider the modifications brought about by the introduction of a rough surface.

In general, when parallel rays are reflected by a rough surface, they undergo changes in path length and amplitude because of the deviations from a smooth reflecting surface. These changes result in a portion of the reflected signal becoming diffuse. Where previously it was totally coherent it now consists of two components: (1) a diffuse component and (2) a coherent component with reduced magnitude.

The reduction to the magnitude of the coherent component brought about by reflections from a rough surface is related to the angle of incidence or grazing angle and the radar wavelength. It is best expressed in terms of the RMS specular scattering coefficient S which is given by[8]

$$S = \exp\left\{-2\left|\frac{2\pi\sigma_H \sin\psi_2}{\lambda}\right|^2\right\}, \tag{38}$$

where σ_H is the rms surface-height variation (assumed normally distributed).

For small values of ψ_2, it is customary to replace $\sin\psi_2$ by ψ_2 and plot S as a function of the 'apparent roughness factor' $\sigma_H\psi_2/\lambda$. A plot of S against $\sigma_H\psi_2/\lambda$ expressed in milliradians is shown in Figure 5.

Beard* has recorded data that shows good agreement with results predicted by eqn. (38) for values of $\sigma_H\psi_2/\lambda \leq 100$ milliradians. However, beyond 100 milliradians, his results, which are shown in Figure 6*, indicates that S decreases more slowly than predicted by theory.

Thus, based on the results of Beard, the specular scattering coefficient given by eqn. (38) is used to determine the magnitude of the coherent component of the reflected signal for values of $\sigma_H\psi_2/\lambda \leq 100$ milliradians. Beyond this value the approximate expression

$$S \cong \exp\left\{-[0.165(\sigma_H\psi_2/\lambda)^2 + 7.42\ \sigma_H\psi_2/\lambda + 0.0468]\right\} \qquad (39)$$

is used. A plot of S against $\sigma_H\psi_2/\lambda$, using eqns. (38) and (39), is shown in Figure 7.

---

* *Beard uses the symbols C/D_r, h and ψ for the parameters identified by S, σ_H and ψ_2 respectively in this report.*

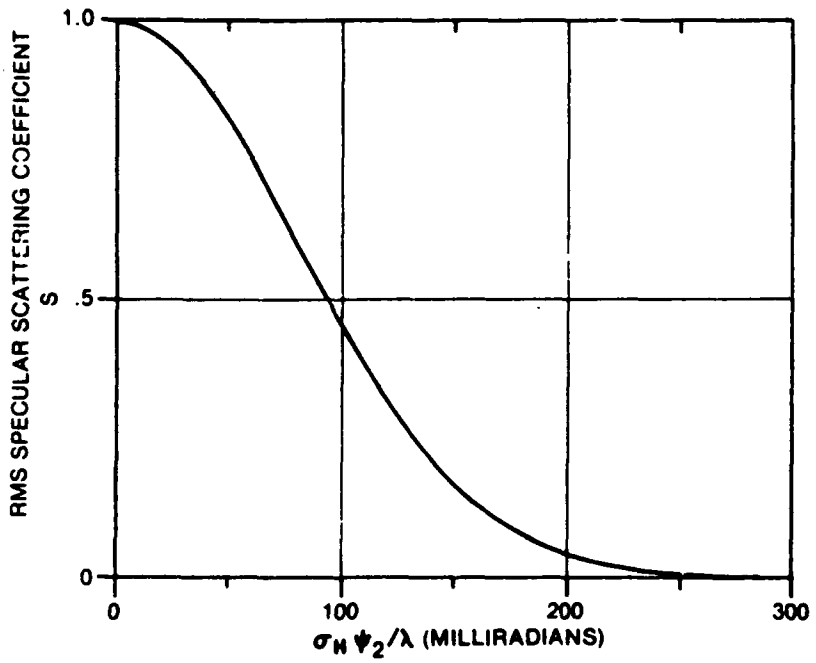

Figure 5. Specular Scattering Coefficient

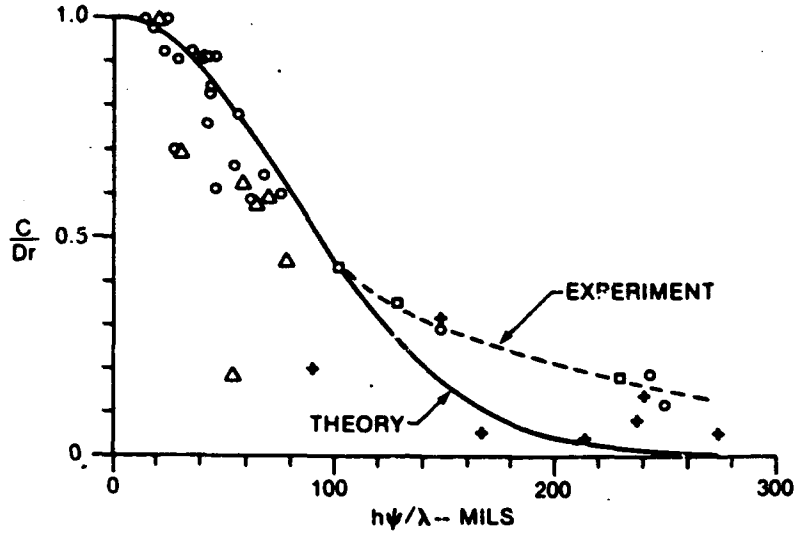

Figure 6. Measured specular scattering coefficient (After: Beard[8])

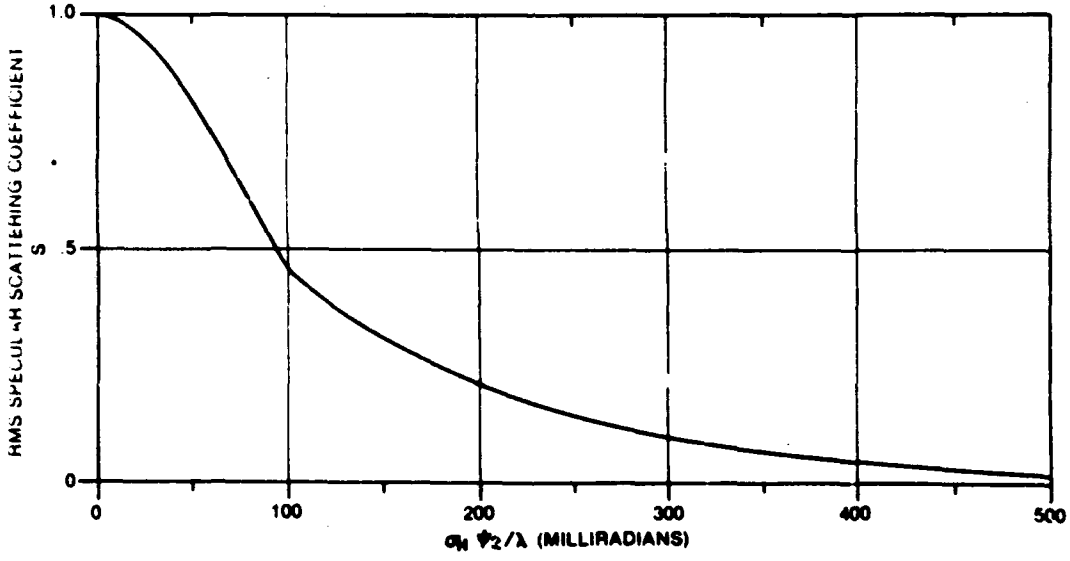

Figure 7. Composite Scattering Coefficient Based on Beard's[8] Results

5.1 RELATIONSHIP BETWEEN SEA-STATE AND σ_H

The parameter used for quantifying the roughness of an ocean surface is called 'sea-state'. It is related to the rms surface height variation σ_H through the 'significant wave height' H. In Nathanson[10] the significant wave height is defined as the average of the highest third of the waves in a wave group and is shown to be related to σ_H by the following:

$$H = 4\sigma_H \ . \tag{40}$$

Thus, if we have an estimate of the sea-state we can, by using eqn. (40) and Figure 7, derive the magnitude of the coherent component of the reflected signal for varying radar-target geometries. In Table 2 is given a list of sea-state numbers (SS) with corresponding values of significant wave height (H).

TABLE 2

Relationship Between Sea-state and Significant Wave Height

Description of Sea	Sea-State (SS) Number	H Metres
Calm	0	0.0
Smooth	1	0.1
Slight	2	0.4
Moderate	3	0.8
Rough	4	1.6
Very Rough	5	3.0
High	6	4.9

6. DERIVATION OF THE SIGNAL AT z_1 FOR A CURVED ROUGH SURFACE

In the discussion in Sections 4 and 5 a number of new parameters were introduced to describe a curved-earth geometry and reflection from a rough surface. These quantities are as follows:

(1) $\Delta r \cong 2z_1'z_2'/r$ - curved-earth path-length difference.

(2) D - divergence factor, to describe defocussing by a curved surface.

(3) S - specular scattering coefficient, to quantify the coherency of the signal reflected by a rough surface.

(4) $Se^{-j\Phi}$ - reflection coefficient, as modified by a rough surface.

By direct substitution into eqn. (10) using the items listed above it follows that:

[redacted]

$$E = 1 + \rho DS\, e^{-j\alpha} \tag{41}$$

where

$$\alpha = \phi + k\Delta r. \tag{42}$$

Equation (41) describes the interference pattern at z_1 resulting from the superposition of the direct signal and the coherent component of the reflected signal. In its description it includes the effects of a curved-earth geometry and reflections from a rough sea-surface.

Figure 8 gives a plot of the amplitude and phase of the interference pattern (E) as a function of z_2 for z_1=4.8m, SS=0 and r=7000m. It should be noted that the interference pattern is periodic in z_2 with a period of about 26.7m. Another interference pattern is given in Figure 9 - this time plotted versus range for the fixed conditions z_1=4.8m, z_2=10m and SS=0. Both Figures 8 and 9 were derived using eqn. (41). Rough-sea results would be similar to these except for a reduced amplitude and a reduction in the phase deviation due to the effect of the factor S in eqn. (41).

7. THE SAMPLED APERTURE

The sampled aperture concept, as implied by its name, entails sampling the amplitude and phase of a complex wavefront at N discrete points along a finite straight line in space (antenna aperture). Using two-dimensional Fourier processing it is possible to develop N independent beams and track up to N targets. The far ranging capabilities of sampled-aperture techniques

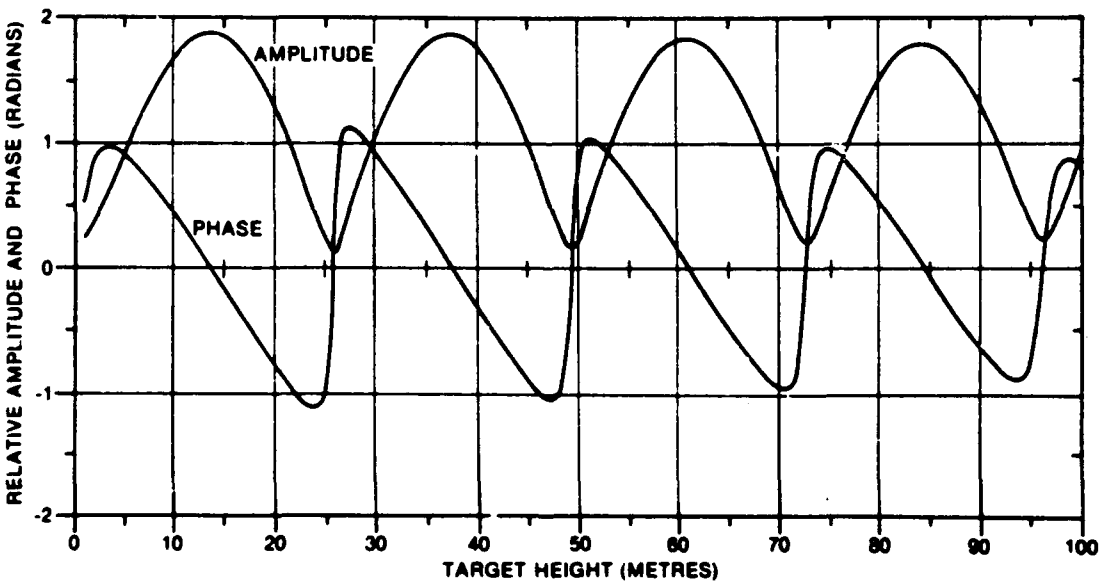

Figure 8. Interference Pattern Phase and Amplitude for a Smooth Sea; z_1 = 4.8m, r = 7000.0m.

[redacted]

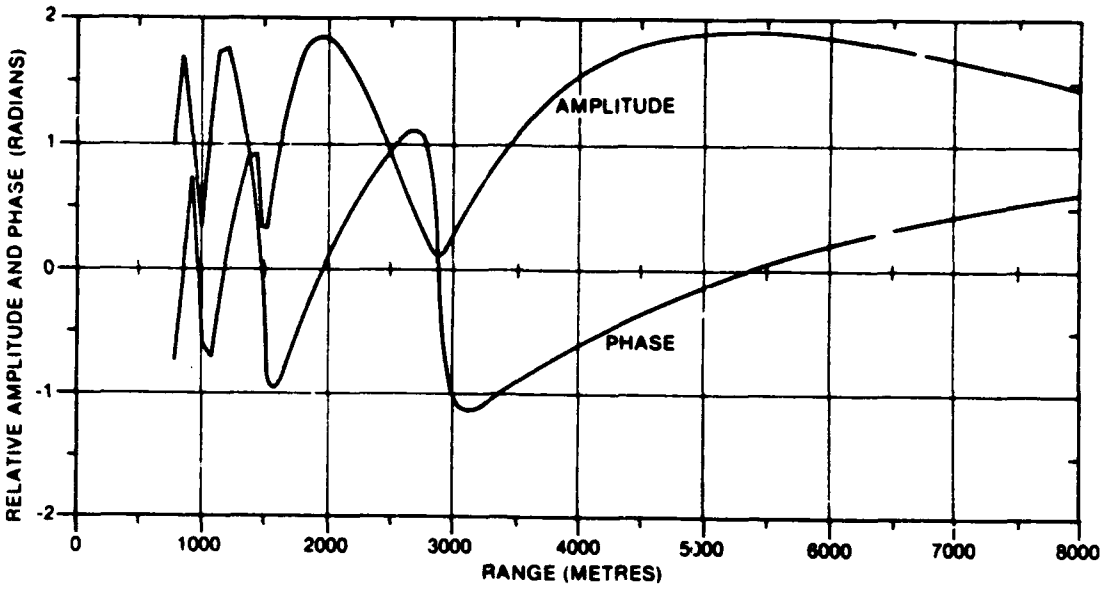

Figure 9. Interference Pattern Phase and Amplitude for a Smooth Sea; z_1 = 4.8m, z_2 = 10.0m.

form a compelling reason for applying this technology to low-angle tracking. Although a full description of possible applications is beyond the scope of this report, expressions will be developed for limited applications. An example of the latter is the use of a sampled-aperture radar to simulate a standard fire-control radar, a use which might be considered to occupy the lowest rung of possible applications.

Consider the linear array shown in Figure 10 consisting of N equally-spaced elements separated by d. It is convenient to consider arrays consisting of odd numbers of elements; with an odd number, the centre of the array coincides with an antenna element which is labelled n=0. With this arrangement, there are (N-1)/2 equal elements on either side of the centre of reference element. If a signal arrives at angle θ relative to the array boresight, then the electric field distribution along the array is

$$E(n) = e^{j(\omega t+kndsin\theta)} \tag{43}$$

where the amplitude is assumed to be unity.

Consider now that the boresight of the array is parallel to the horizontal plane in Figure 4 (i.e., $\theta_p \equiv 0$), recalling that the uppermost element is n = (N-1)/2, and that the direct and indirect signals arrive at angles θ_d and θ_i respectively, then the amplitude and phase distribution of the composite signal across the array is

$$E(n) = E_d(n)+E_i(n) = \left[e^{jkndsin\theta_d} + e^{jkndsin\theta_i}\right]e^{j\omega t}, \tag{44}$$

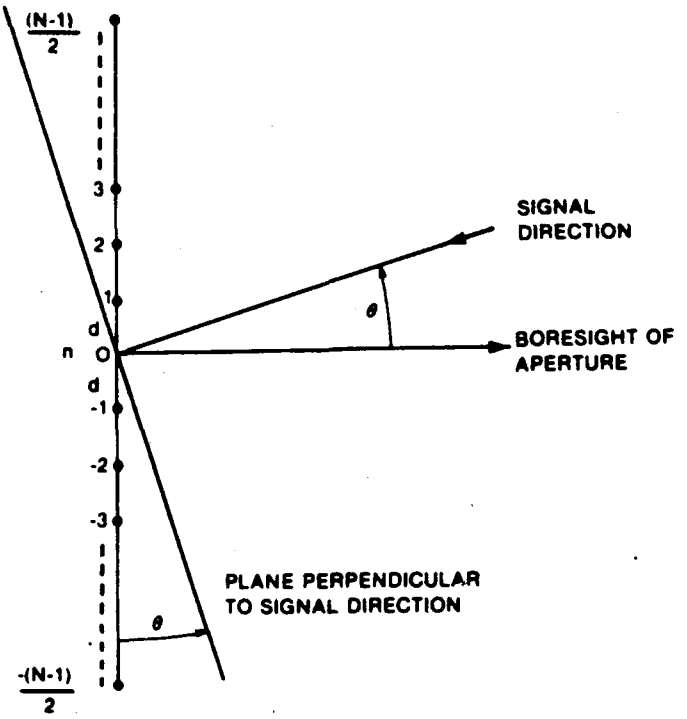

Figure 10. Sampled Aperture Geometry

where both signal amplitudes are set equal to one and the phase-path difference between the direct and indirect signals at the reference element is assumed equal to zero. As before, only that portion of eqn. (44) within the square brackets is of interest to us, therefore, we retain this portion and discard the remainder, giving

$$E(n) = e^{jkndsin\theta_d} + e^{jkndsin\theta_i}. \tag{45}$$

We now wish to incorporate into eqn. (45) the parameters, ρ, D, S and α which, for a given r and z_2, are derived soley for a value of z_1 which corresponds to the reference element (n=0). For all other n, the computed values of ρ, D, S and α may be regarded as being approximately equal to those computed for n=0 since the separation of the elements of the array is small compared to r_1 in Figure (4). When eqn. (45) is rewritten to incorporate the above parameters and to reflect its dependence on n, r, and z_2, it takes the form

$$E(n,r,z_2) \cong e^{jkndsin\theta_d} + A(o,r,z_2)e^{-j[\alpha(o,r,z_2)-kndsin\theta_i]}, \tag{46}$$

where for convenience

$$A(o,r,z_2) = \rho(o,r,z_2)\cdot D(o,r,z_2)\cdot S(o,r,z_2). \tag{47}$$

Alternatively, eqn. (46) may be expressed in polar form with amplitude and phase of the resultant given respectively by

$$|E(n,r,z_2)| \cong \left\{1 + 2A(o,r,z_2)\cos[knd(\sin\theta_d-\sin\theta_i) + \alpha(o,r,z_2)] + A^2(o,r,z_2)\right\}^{1/2} \quad (48)$$

and

$$\phi(n,r,z_2) \cong \tan^{-1}\left[\frac{\sin(kndsin\theta_d)-A(o,r,z_2)\sin[\alpha(o,r,z_2)-kndsin\theta_i]}{\cos(kndsin\theta_d)+A(o,r,z_2)\cos[\alpha(o,r,z_2)-kndsin\theta_i]}\right]. \quad (49)$$

When n=0,

$$|E(o,r,z_2)| = \left\{1 + 2A(o,r,z_2)\cos[\alpha(o,r,z_2)] + A^2(o,r,z_2)\right\}^{1/2} \quad (50)$$

and

$$\phi(o,r,z_2) = \tan^{-1}\left[\frac{-A(o,r,z_2)\sin[\alpha(o,r,z_2)]}{1 + A(o,r,z_2)\cos[\alpha(o,r,z_2)]}\right]. \quad (51)$$

It follows from eqns. (48)-(51) that the amplitude and phase distribution across the aperture after normalization by the amplitude and phase at the reference element is

$$F(n,r,z_2) = \left|\frac{E(n,r,z_2)}{E(o,r,z_2)}\right| \underline{/\phi(n,r,z_2)-\phi(o,r,z_2)}. \quad (52)$$

It will be noted in eqn. (52) that when n=0, $F(n,r,z_2)$ reduces to unity and the corresponding phase is zero. This equation is important because it gives the resultant normalized phase and amplitude distribution of a composite wavefront whose components consist of the direct and indirect signals arriving from a low-angle target located at (r,z_2).

In the development of formulae to describe the relative phase and amplitude observed at z_1 due to two signals (see eqn. (4)), it was only necessary to consider the quantity which described the interference pattern. Thus, the remaining factor was discarded for ease of manipulation and clarity in subsequent mathematical development. In any event, if this factor had been included throughout the development, it would have finally disappeared at this point due to the normalization procedure described by eqn. (52). In addition, this procedure effectively reduces the dependency of $F(n,r,z_2)$ on range and target cross-section.

The choice of the reference element in the aperture is completely arbitrary subject to the constraint of there being an equal number of

[redacted]

elements on either side of the reference. One can, for example, divide the array into smaller segments consisting of odd numbers of elements. This allows sampling the wavefront for different values of z_1, where z_1 is the height of the centre element of the array segment. It will be shown in Section 8 that this flexibility can be used as a basis for a technique for resolving target height ambiguities which result when low-angle data are processed by the CHA filter.

Although the sampled-aperture technique has been discussed for a specific application i.e., the low-angle tracking problem, one is at liberty to process the data in a variety of ways. For example, beamforming studies could be carried out using the discrete Fourier transform[11], White's[12] double null technique or adaptive array processing[13]. It is thought that the possibilities for processing sampled-aperture data are virtually boundless and probably only limited by one's imagination.

8. COMPLEX CORRELATION COEFFICIENT

When tracking a low-angle target with a sampled-aperture radar, the target range and antenna height can be considered to be known parameters. The unknown is z_2 and it is our intent to solve for z_2 by cross-correlating experimental data with simulated data.

Let us define the measured value of the signal at element n to be $W(n,r)$. Its normalized value $T(n,r)$ is then given by

$$T(n,r) = \left|\frac{W(n,r)}{W(o,r)}\right| \underline{/\phi(n,r)-\phi(o,r)} \quad , \tag{53}$$

where $|W(n,r)|$ and $\phi(n,r)$ are the values of amplitude and phase measured at element n. When expressed in complex notation, eqn. (53) becomes

$$T(n,r) = \left|\frac{W(n,r)}{W(o,r)}\right| e^{j\left\{\phi(n,r)-\phi(o,r)\right\}} . \tag{54}$$

For a given value of r, simulated data may be calculated for various values of z_2 from eqn. (52). Expressed in complex notation, eqn. (52) becomes

$$F(n,r,z_2) = \left|\frac{E(n,r,z_2)}{E(o,r,z_2)}\right| e^{j\{\phi(n,r,z_2)-\phi(o,r,z_2)\}} . \tag{55}$$

The technique used in solving for z_2 consists of deriving cross-correlation coefficients for the measured amplitude and phase distribution across the array aperture, for a particular r, with simulated data calculated for closely spaced values of z_2. Peaks in the cross-correlation coefficient are used to define possible values for the target height z_2. Typically, z_2 is sampled at 1m intervals for a total of about 100 samples. After the measured and simulated data are correlated the number of possible target heights may be reduced to 10.

[redacted]

Using the general expression given in Litva[1] the complex correlation coefficient, denoted by C, may be written in terms of r and z_2 as

$$C(r,z_2) = \sum_{-(N-1)/2}^{(N-1)/2} T(n,r)F^*(n,r,z_2)/\sigma(r)\cdot\sigma(r,z_2), \tag{56}$$

where

$$\sigma(r) = \left\{ \sum_{-(N-1)/2}^{(N-1)/2} T(n,r)T^*(n,r) \right\}^{1/2} \tag{57}$$

and

$$\sigma(r,z_2) = \left\{ \sum_{-(N-1)/2}^{(N-1)/2} F(n,r,z_2)F^*(n,r,z_2) \right\}^{1/2} . \tag{58}$$

and * denotes the complex conjugate. It should be noted that the complex correlation coefficient given by eqn. (56) is calculated over all N spatially sampled points, where N is the total number of antenna elements or a subset of that number in the case where the array is segmented into sub-arrays.

In the following sub-section, examples of the complex correlation coefficient, using simulated data, are presented and examined.

8.1 DISCUSSION OF SIMULATED RESULTS

The results to be presented in this section were derived using simulated data for a sampled aperture consisting of seven elements with an inter-element spacing d of 0.128m (4λ). The boresight of the aperture is assumed to be parallel to the horizontal plane (i.e., θ_p=0) with z_2=10m, r=7000m and SS=0. At this stage of the development of the CHA algorithm only the real part of the complex correlation coefficient is considered. Further studies involving the imaginary part will be carried out at a later date.

Figure 11 gives the real part of the complex correlation coefficient, $R[C(r,z_2)]$, as a function of z_2. This result was derived using all seven elements of the sampled aperture, whereby N=7 and z_1=4.8m, where, it will be recalled, z_1 gives the height of the reference element.

It is noted that $R[C(r,z_2)]$ repeats periodically with increasing z_2, which is consistent with the behavior of the interference pattern given in Figure 8. In addition, the maxima of the correlation peaks gradually decrease with increasing values of the index K, where K identifies the correlation peaks. The true peak is given by K=0 and the false or alias peaks by K>0. In Figure 11, one can see the difficulty in distinguishing the true peak from the adjacent peaks simply on the basis of its size.

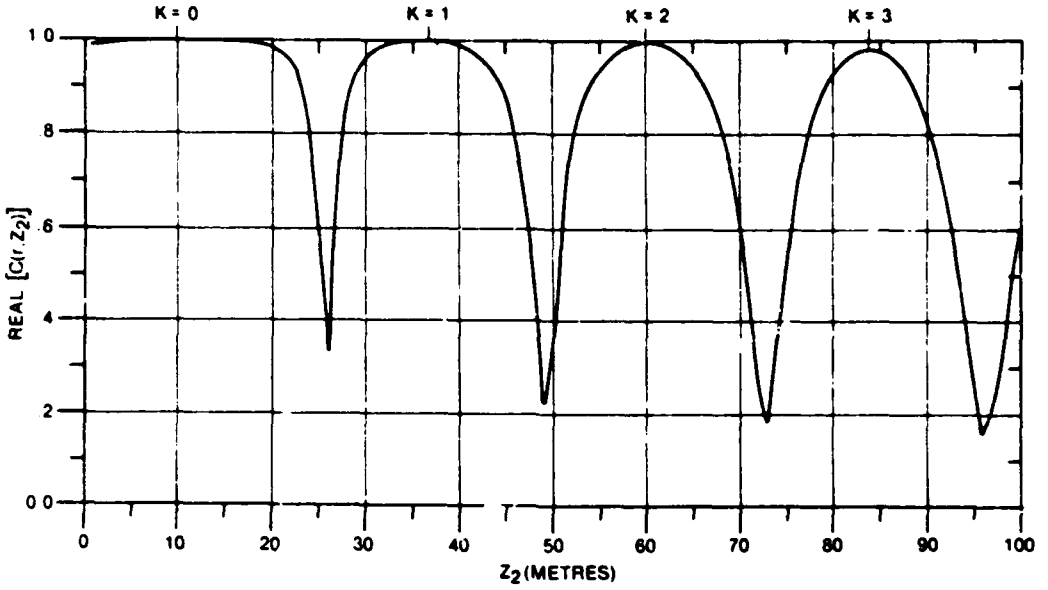

Figure 11. Synthetic Cross-correlation coefficient; z_1 = 4.8m, z_2 = 10.0m, N = 7, θ_0 = 0.0mr, r = 7000.0m.

In general, the size of the correlation peaks does not form a particularly good criterion for selecting the true peak. The rate of decrease of the maxima for increasing K relies heavily on the ratio of the aperture length to the scale length of the interference pattern. This point is brought out in Figure 12, where only the uppermost three elements (N=3) are used in deriving the complex correlation coefficient. For this result z_1 = 5.056m. One sees that the fall-off in the maxima of the peaks is much more gradual and it has become more difficult to distinguish the peak having the largest value.

Whereas, selection of the true peak on the basis of its maximum value is unreliable, the magnitudes of the peaks can be used as a criterion to reduce the number of alias tracks. A reference level can be set and peaks can be excluded on the basis of their maxima falling below the reference level. As an example of this, Figure 13 shows four target tracks, the true track identified by K=0 and three alias tracks identified by K=1, K=2, and K=3; these tracks were selected on the basis of the maxima of their correlation peaks exceeding 0.8. All remaining alias tracks have maxima that fall short of 0.8 and are rejected on that basis.

It is noted that the alias tracks converge to the true track, i.e., z_2=10m, at r=0m. This behavior illustrates the decrease in the scale length of the interference pattern for decreasing range. It follows that if r is decreased in Figure 11, then the peaks will crowd together.

These results corroborate some of the basic elements of the CHA technique, namely;[1] (1) a family of target tracks are generated when simulated and measured data are cross-correlated; (2) one of the tracks is the true

target track and the remainder are false or alias tracks. Although the true target track cannot be selected unambiguously on the basis of the magnitudes of the correlation peaks, the majority of the alias tracks can be rejected by ranking the correlation peaks according to size.

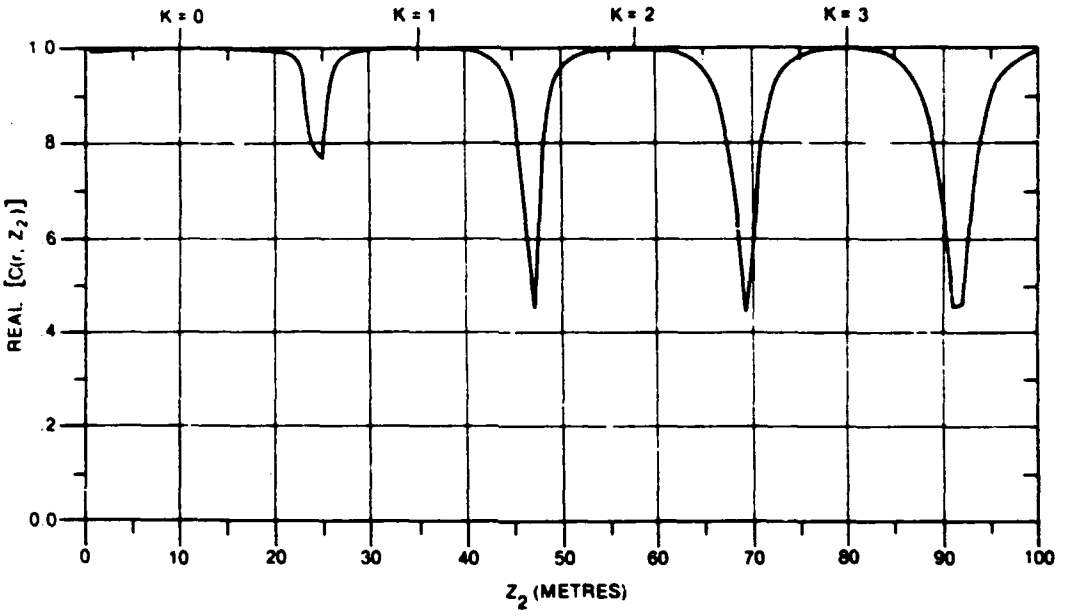

Figure 12. Synthetic Cross-correlation coefficient; z_1 = 5.056m, z_2 = 10.0m, N = 3, θ_p = 0.0mr, r = 7000.0m.

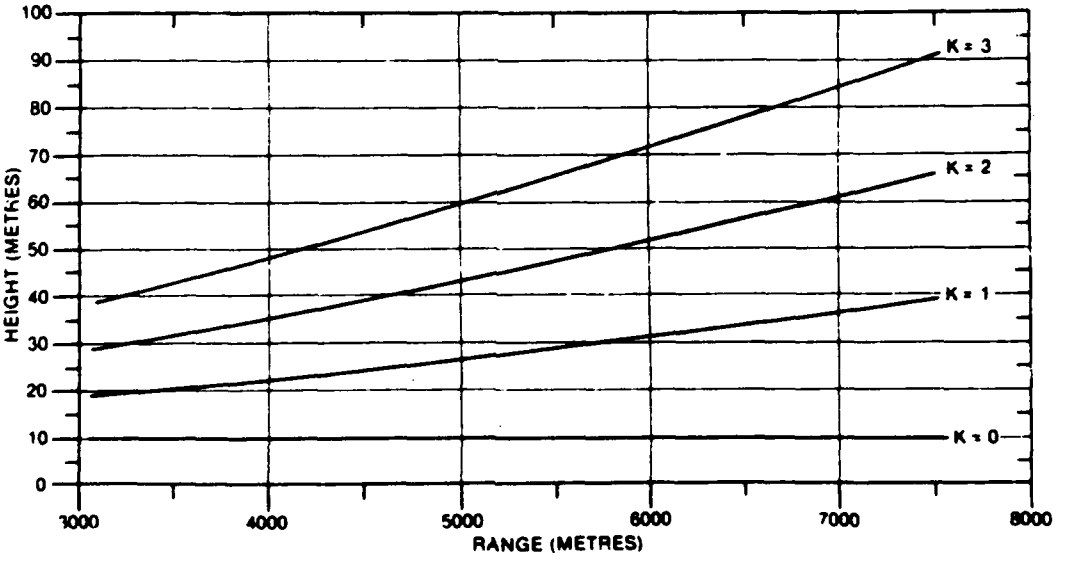

Figure 13. Synthetic CHA Target Tracks; z_1 = 4.8m, z_2 = 10.0m, θ_p = 0.0mr, N = 7.

9. IDENTIFICATION OF THE TRUE TARGET TRACK

It has been shown that a family of target tracks can be derived by correlating measured data with theoretical data. The issue that now needs to be addressed is that of identifying the true target track.

In Ref. 1, Litva showed by means of analysis that if the radar frequency and/or antenna height were perturbed in a known manner, deviations, exhibiting similar characteristics, would appear on all the tracks except for the true track. He did not support his results with experimental data but gave an expression which relates the magnitude of the deviations as a function of frequency and/or height perturbations; namely

$$\Delta H_K = (K-K_T)\Delta H\left\{\frac{\Delta f}{f} + \frac{\Delta z_1}{z_1} + \frac{\partial J}{\partial z_1}\cdot\frac{\Delta z_1}{J}\right\}r \qquad (59)$$

where $(K-K_T)$, which takes on both positive and negative values, identifies the order of the track relative to the true track of number K_T, and

$\Delta H = \frac{\lambda}{2z_1 J}$,

$\frac{\Delta f}{f}$ = the relative change in the radar frequency,

$\frac{\Delta z_1}{z_1}$ = the relative change in the antenna height, z_1 being its average height,

$\frac{\partial J}{\partial z_1}\cdot\frac{\Delta z_1}{J}$ = a quantity which only becomes significant for very low target heights, and

J = a curved earth correction factor.

From Appendix A of Ref. 1, an expression for J in terms of z_1, z_2 and A_e is given as

$$J = \left[1 - \frac{r_1^2}{2A_e z_1}\right]\left[1 - \frac{r_2^2}{2A_e z_2}\right] \quad . \qquad (60)$$

It follows from eqn. (59) that the sign of ΔH_K reverses when going from an alias track with $(K-K_T) > 0$ to one with $(K-K_T) < 0$.

Equation (59) can be simplified by: (1) restricting our discussion to small values of r, where the flat-earth approximation can be used so that $J \cong 1$ and $\partial J/\partial z_1 \cdot \partial z_1/j << \Delta z_1/z_1$ and (2) keeping f constant, whereby $\Delta f/f=0$. With these approximations,

$$\Delta H_K \cong \frac{(K-K_T)\lambda}{2z_1} \cdot \frac{\Delta z_1}{z_1} \cdot r. \qquad (61)$$

If the approximations leading to eqn. (61) are valid, it follows that for a given relative change in the antenna height $\Delta z_1/z_1$ and constant r, the magnitude of the deviations on the K^{th} track is a linear function of K. From both eqn. (59) and its approximation, eqn. (61), it follows that for $K=K_T$, $|\Delta H_K| \equiv 0$.

Earlier in our discussion we saw that the use of a sampled-aperture radar provided a built-in capability for perturbing the effective antenna height. This is accomplished by varying N or dividing the array into subarrays. Therefore, the means for demonstrating track resolution is at hand.

9.1 DISCUSSION OF SIMULATED RESULTS

In this section, simulated results are presented to illustrate the antenna-height perturbation technique for identifying the true track. The sampled-aperture and sea-state parameters listed in Section 8.1 also apply to the results presented here.

Figure 14 gives $R[C(r,z_2)]$ for two antenna heights with r=7000m. These two heights were achieved by partitioning the array into two sub-arrays with the uppermost five elements used for one array and the lowermost five elements for the other. This gave effective antenna heights of $z_1^U = 4.928$m and $z_1^L = 4.672$m, where the superscripts U and L denote uppermost and lowermost respectively. With the exception of the peak, K=0, all the peaks undergo a displacement when the antenna heights are switched and the magnitude of this displacement increases as K increases. A similar result is obtained if only the three uppermost (N=3) and three lowermost elements are used. These results are given in Figure 15 where in this case z_1^U and z_1^L were 5.056 and 4.544m respectively.

The magnitudes of the displacements in Figure 15 are considerably larger than those in Figure 14 because; (1) the relative effective-height variation is about twice as large; and (2) the effect of J in eqn. (59). The approximations leading to eqn. (61) are not accurate in describing these results because z_1 and z_2 are both small. Therefore, the curved earth correction parameter J must be retained. For an accurate description of the magnitude of the deviations in Figures 14 and 15 one must return to eqn. (59).

If now the results are given in terms of range, where target height is used in place of the correlation coefficient for the dependent variable, we have the results shown in Figures 16 and 17. These correspond to the cases N=5 and N=3, respectively. Except for the magnitudes of the deviations, these two results are similar. Deviations appear on all tracks except for the true track (K=0); their magnitudes increase with increasing K and decrease with decreasing r.

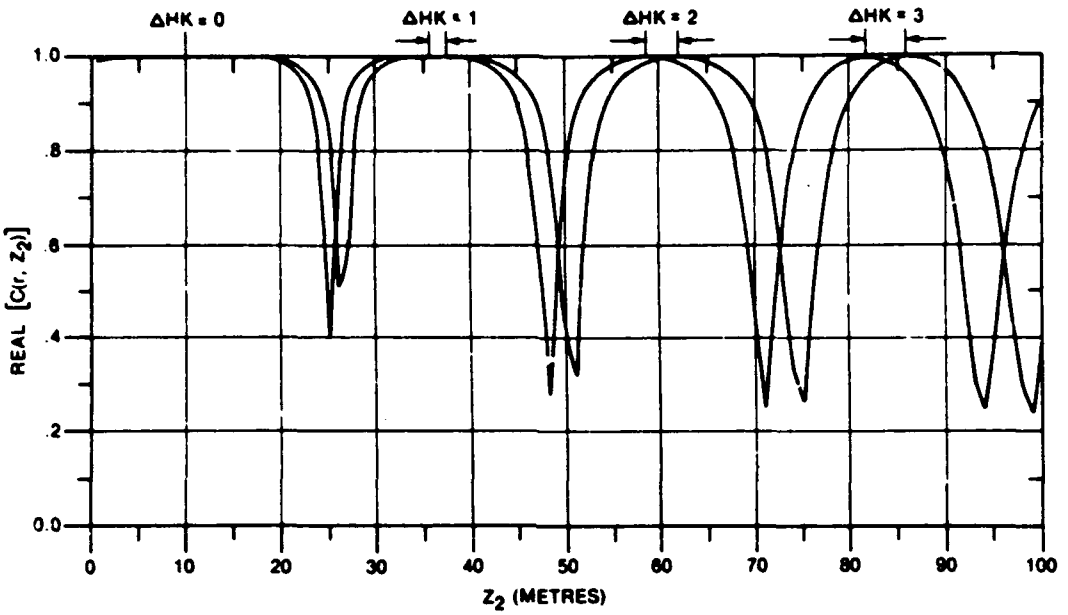

Figure 14. Synthetic Cross-correlation Coefficients; $z_1^U = 4.928m$, $z_1^L = 4.672m$, $N = 5$, $\theta_p = 0.0mr$, $r = 7000.0m$.

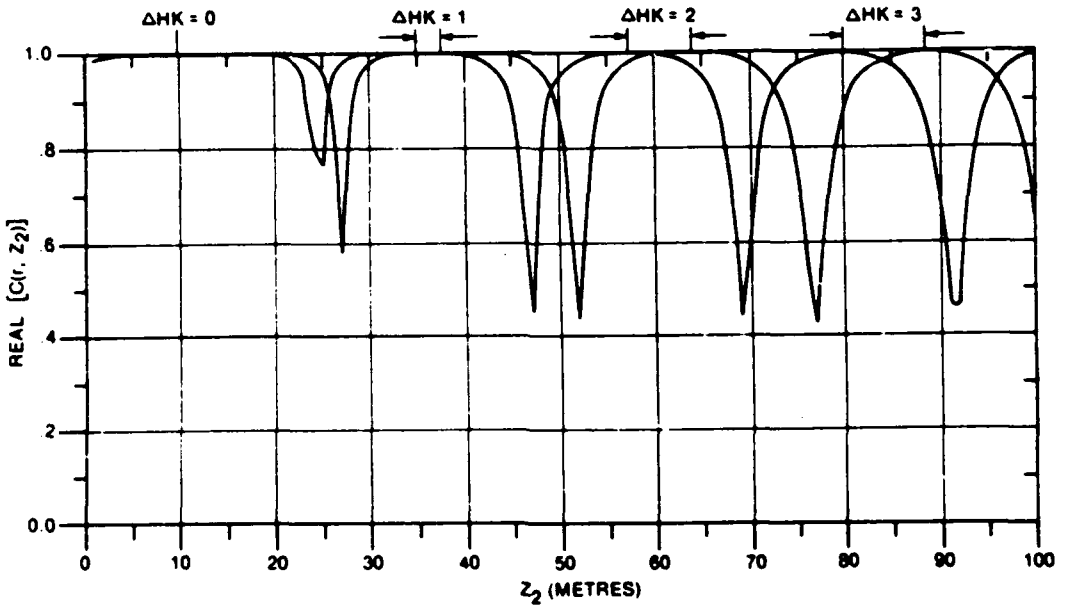

Figure 15. Synthetic Cross-correlation Coefficients; $z_1^U = 5.056m$, $z_1^L = 4.544m$, $N = 3$, $\theta_p = 0.0mr$, $r = 7000.0m$.

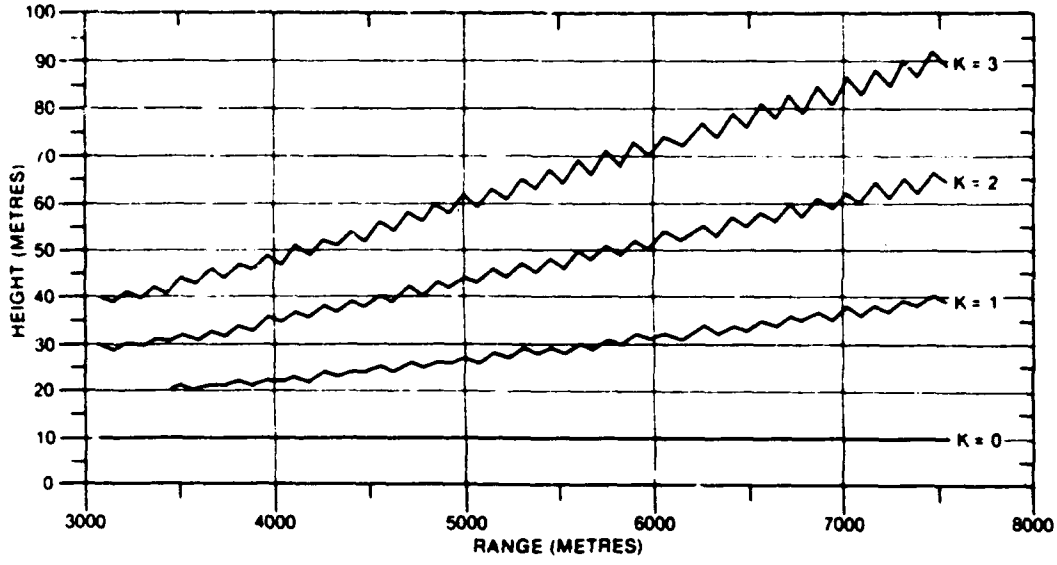

Figure 16. Synthetic CHA Target Tracks; $z_1^U = 4.528m$, $z_1^L = 4.672m$, $N = 5$, $\theta_p = 0.0mr$, $K_T = 0$.

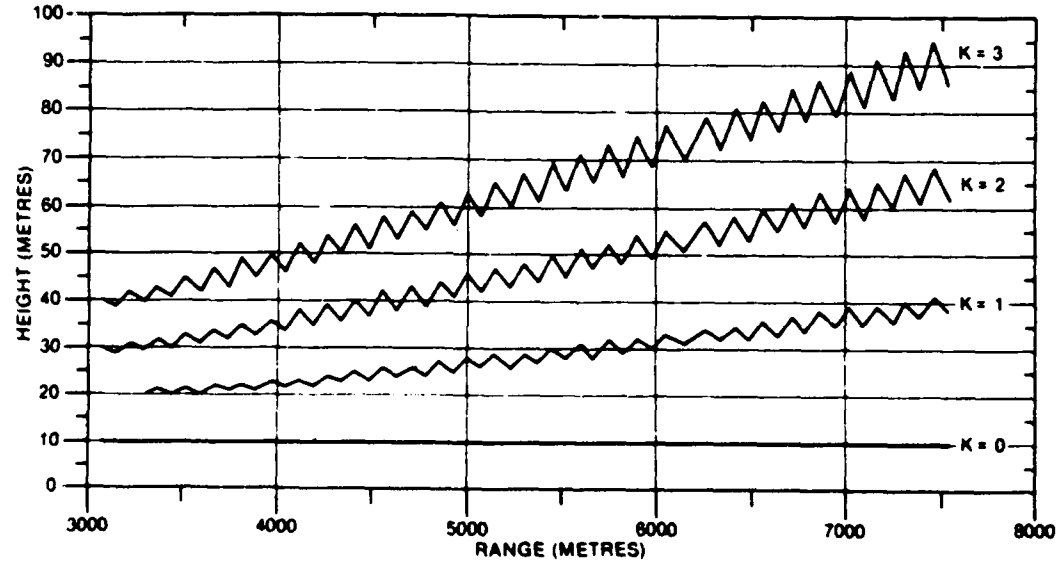

Figure 17. Synthetic CHA Tracks; $z_1^U = 5.056m$, $z_1^L = 4.544m$, $N = 3$, $\theta_p = 0.0mr$, $K_T = 0$.

As a demonstration of the effect of J in eqn. (59) and the errors incurred in setting J=1 in eqn. (61), let us consider a particular example. Before doing so, it should be pointed out that one would expect J to depart from unity under conditions of increasing r and decreasing z_2 simply because the earth's curvature becomes more apparent. In our example z_1=4.2m and z_2=10m. When r=7500m, J and $\partial J/\partial z_1$ are 0.805 and 1.376 x 10^{-2} m^{-1} respectively. For these values the magnitude of $\partial J/\partial z_1 \cdot \Delta z_1/J$ is only about one-tenth that of $\Delta z_1/z_1$ in eqn. (59) and therefore justifiably considered to be negligible. The error in $|\Delta H_k|$ resulting from the approximation J=1 is about 20%. As r decreases, the ratio of $\Delta z_1/z_1$ to $\partial J/\partial z_1 \cdot z_1/J$ increases and J approaches more closely to unit. Therefore, the approximations made in eqn. (61) become more exact. For example, when r is reduced to 3500m, J becomes 0.95 and the error incurred in setting J=1 is reduced to 5% and the error in neglecting $\partial J/\partial z_1 \cdot \Delta z_1/J$ becomes even less than at r=7500m.

In comparing Figures 16 and 17 one sees that the ease of selecting the true track is enhanced as $\Delta z_1/z_1$ is increased. When the CHA low-angle filter is used with a radar for tracking low-angle targets, it is necessary that $\Delta z_1/z_1$ or $\Delta f/f$ be chosen sufficiently large so that the track deviations are detectable above the noise. For high noise environments, it may be necessary to implement matched filtering by correlating the noisy track deviations with a replica of the expected deviations.

10. EXPERIMENTAL ARRANGEMENTS

The experimental data to be presented in this section are not only intended to demonstrate the CHA technique, but also to highlight some particular aspects, such as the track identification technique described in the previous section.

For this purpose a series of experiments were conducted over an area of the Ottawa River shown in Figure 18 using an experimental sampled-aperture array. The array consisted of seven elements, the beamwidths of which were approximately 28°, with an inter-element spacing of d=0.128m (4λ). The beam maxima of all the elements were aligned in the boresight direction of the array. Each element was connected to its own receiver, the local oscillator signal was provided by a common oscillator. In this way the phase relationship between the signals at the antenna terminals were preserved in the I and Q signals appearing at the outputs of the receivers. Range information was provided by a Furuno radar which together with the sampled-aperture array formed the experimental radar facility.

A boat equipped with a mast which has a CW source attached to it, was used to simulate low-angle targets. The source, which emitted a vertically polarized signal at 9.375 GHz, was adjustable in height over a range from 5 to 10m above the surface of the water. An Alpine transponder located on the same mast was used in conjunction with the Furuno radar to provide accurate radar range information.

The experimental radar facility, which is housed in a trailer, was located at the point shown in Figure 18. The boresight of the aperture was pointed down the range towards Breckenridge. The facility was under

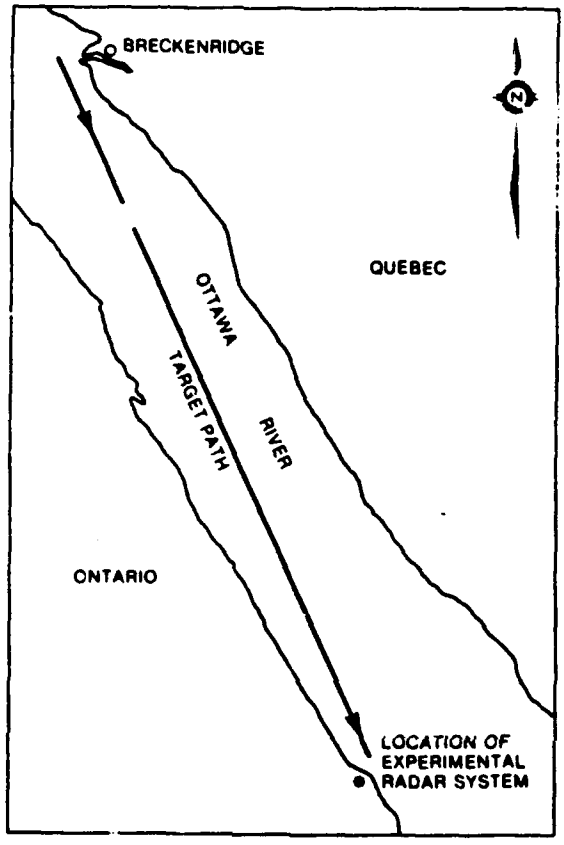

Figure 18. Site of Low-angle Measurements

computer control whereby the radar range together with phase and amplitude (I,Q) information were sampled, digitized and recorded on magnetic tape for processing at a later date. Further information on the experimental arrangements and the characteristics of the sampled-aperture facility including its detection sensitivity in the low-angle region, will be discussed in a report to be published later.

A series of experiments were conducted whereby data were recorded for various constant target heights over a radar range from approximately 8000m to 500m. From the results of these experiments, three have been selected as being representative of the complete series and are presented in the following sub-section. However, before proceeding to this section, a list of the parameters which were common throughout these experiments are as follows:

$z_1 = 4.8m$

$SS = 1$

$\theta_p = -12.0$ milliradians

[redacted]

It was intended that the axis of the array to be coincident with the vertical (i.e., $\theta_p \equiv 0$), however, it was found that θ_p was decremented by 12.0 milliradians relative to the horizontal line. This decrement was due to a combination of the trailer not being level and the sloping terrain over which the experiments were conducted.

10.1 DISCUSSION OF EXPERIMENTAL RESULTS

Figures 19 and 20 give the amplitudes recorded at two of the array's elements for a target height of 7.39m. They have not yet been normalized by the amplitude recorded at a reference element. These results illustrate classical interference patterns - in this case, those appropriate to antenna heights 5.18m and 4.42m respectively.

It is noted that the period of the interference pattern decreases with decreasing range in accordance with the theoretical results described previously.

Comparing Figures 19 and 20 one observes a strong dependence of the position of the peaks and troughs of the interference patterns on antenna height. This demonstrates the high sensitivity obtained by using the sampled-aperture technique for deriving target heights by spatial sampling of the interference patterns.

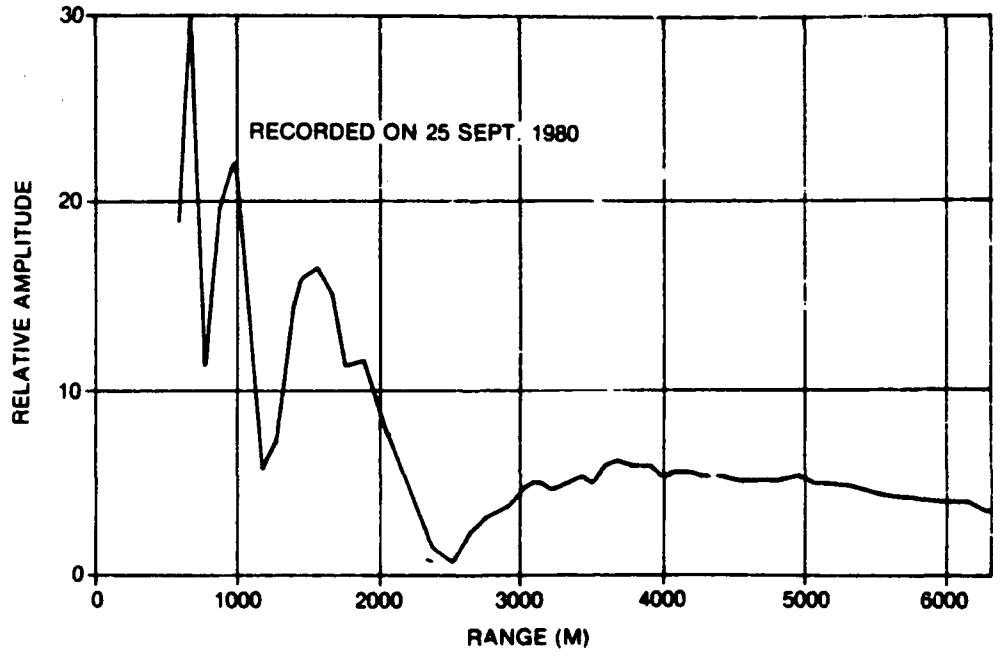

Figure 19. Measured Signal Amplitude on Element 1; z_1 = 5.18m, z_2 = 7.39m, θ_p = -0.012 radians, λ = 0.032m.

[redacted]

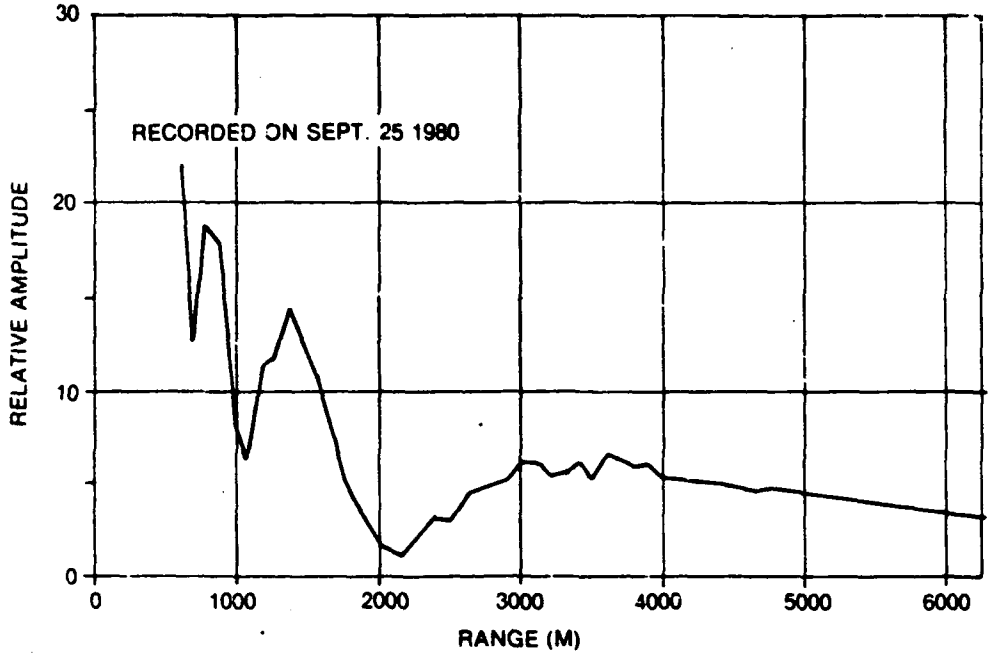

Figure 20. Measured Signal Amplitude on Element 7; z_1 = 4.42m, z_2 = 7.39m, θ_p = -0.012 radians, λ = 0.032m.

The first CHA result to be presented is given in Figure 21. It was derived using the same data set from which the examples in Figures 19 and 20 were taken. The measurements, which were taken at increments of approximately 2m in range, were averaged over 50 data points prior to processing in the CHA filter. The data has been subjected to some correction for longer term drift and instabilities in the sampled-aperture array. In other words, it has been corrected for measurement errors that would normally be accounted for by careful and frequent calibration of the radar system. The procedure used for correcting the data will be described in more detail in a subsequent report. The track deviations were obtained by switching, during the course of the CHA processing, from the uppermost three to the lowermost three elements. The corresponding reference element heights were z_1^U = 5.06m and z_1^L = 4.54m.

It should be noted that the results are, in general, similar to the simulated results presented earlier. Although there are deviations on the true track, they are clearly smaller than those appearing on the alias tracks, therefore, the true track is easily identified. The deviations appearing on the true track are probably due to inaccuracies in calibration and noise. Additional CHA results are given in Figures 22 and 23 for target heights of 5 and 10m. They are similar to Figure 21 and equally consistent with simulated results.

In the model which was used for deriving simulated data, the fact that the data were recorded over fresh-water rather than sea-water was taken into account by using appropriate values of ϵ/ϵ_o and σ from Table 1 for computing

the reflection coefficient. Furthermore, the array elements were assumed to be isotropic point receivers. This is a reasonable assumption since, in the low-angle region, the angles-of-arrival of the direct and indirect signals are small compared with the beamwidth of the elements used in the experimental facility.

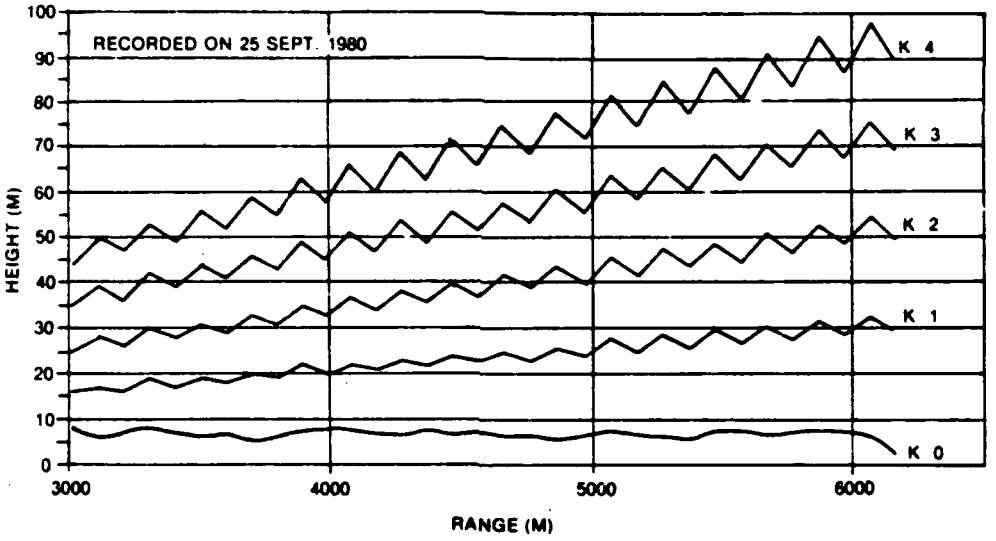

Figure 21. CHA Tracks Obtained From Measured Data; $z_1^U = 5.06m$, $z_1^L = 4.54m$, $z_2 = 7.39m$, $N = 3$, $\theta_p = -0.012$ Radians, $\lambda = 0.032m$, $K_T = 0$.

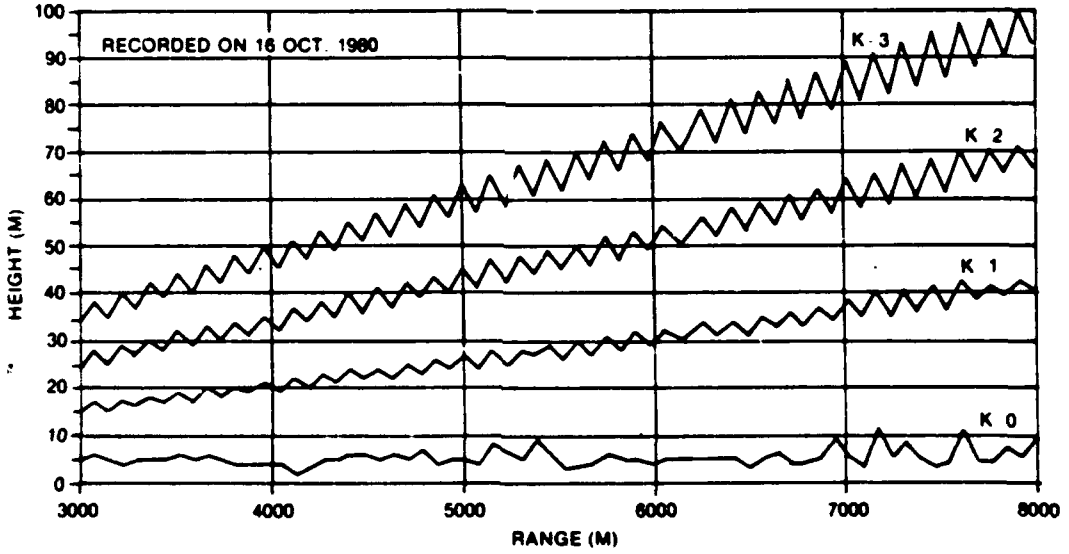

Figure 22. CHA Tracks Obtained From Measured Data; $z_1^U = 5.06m$, $z_1^L = 4.54m$, $z_2 = 5.0m$, $N = 3$, $\theta_p = -0.012$ Radians, $\lambda = 0.032m$, $K_T = 0$.

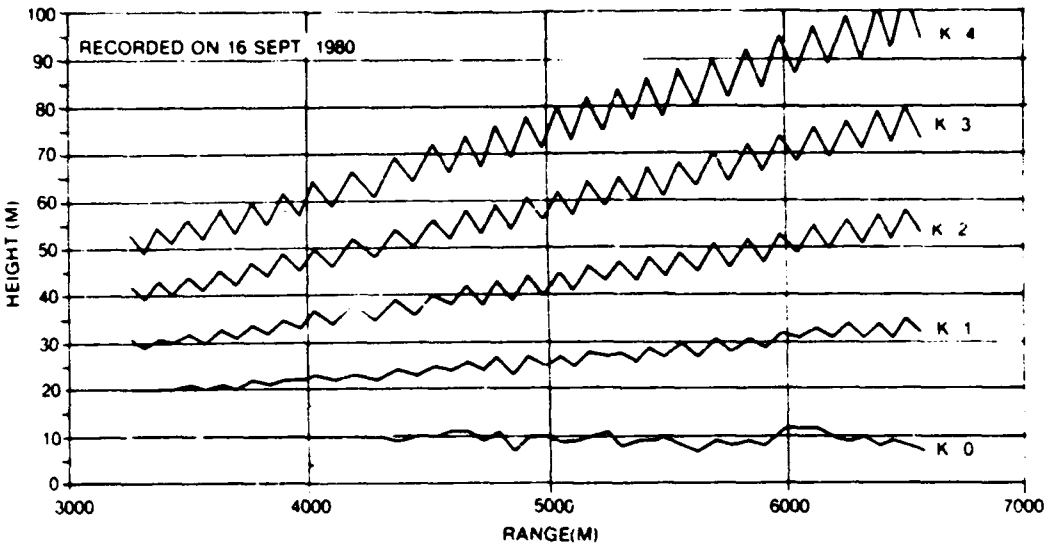

Figure 23. CHA Tracks Obtained From Measured Data; z_1^U = 5.06m, z_1^L = 4.54m, z_2 = 10.0m, N = 3, θ_p = -0.012 Radians, λ = 0.032m, K_T = 0.

11. ALGORITHMIC PROCEDURE FOR TRACK IDENTIFICATION AND DEVELOPMENT

In the previous section it was demonstrated that one could pick out the true target track visually, simply by noting which track had the smallest deviations. We wish now to describe an algorithmic procedure in which identification and subsequent tracking of the target may be carried out automatically in a digital computer.

There are two points to note regarding this procedure, namely; (1) we must have some knowledge of the magnitude of the deviations to be expected at the range of the target and (2) we must always maintain a good profile of the correlation coefficient over the vector comprised of values of z_2.

Implementation of track identification starts with the first measurements of the target range and of the amplitude and phase distribution across the array. At the onset an estimate of the deviations on the first alias track, i.e., $(K-K_T)=1$, is derived by using eqn. (61), which is

$$|\Delta H_K| \cong \frac{\lambda}{2z_1} \cdot \frac{\Delta z_1}{z_1} r \ . \qquad (62)$$

The choice of the initial group of elements or subarray is unimportant, therefore we shall start with the uppermost group. Also, since we have little a priori knowledge at this point of an optimum increment size for z_2, we start with a value of 1m. Beginning at z_2=1m, the complex correlation coefficient is calculated for each incremental value of z_2 until z_2=100m. The values of z_2 (correlated heights) which correspond to peaks in the real

part of the complex correlation coefficient with values that exceed 0.95 are noted and recorded. A new increment size, z_{INC} is derived from the average separation in the correlated heights (z_{AV}), using

$$z_{INC} = \frac{z_{AV}}{20} \quad . \tag{63}$$

New height vectors for z_2, corresponding to a new range, are derived in preparation for the next step in the data processing. These values are computed in the vector range from the lowest correlated height decremented by $z_{AV}/4$ to the highest incremented by $z_{AV}/4$.

In the next iteration, where the lowermost group of elements are used, both z_{AV} and z_{INC} are updated through multiplying these values by the ratio of the present range value to that of the initial range value. The purpose of this update is to take into account the decreasing period of the correlation coefficient in z_2 with decreasing range. In addition, $|\Delta H_K|$ is also updated by multiplying it by the same ratio.

The correlation coefficient is then determined in the manner described previously; the height vectors for which the correlation is a maximum (correlated heights) are noted and compared with the previous ones in order to establish tracks and their respective accumulated track deviations. The previous correlated heights are then replaced with the present ones.

A test is then carried out so that tracks with deviations greater than $|2\Delta H_K|$ can be discarded, thereby further reducing the range of height vectors in the following iteration. In addition, the values of the accumulated deviations are tested to see if one can be considered to be a true minimum. It is only considered to be so if its value is smaller, by at least $|\Delta H_K|$, than any of the other accumulated track deviations. The process described above is repeated until the true track has been identified.

Once the true target height, and thus the true target track has been identified, a range of height vectors $\pm z_{AV}/4$ centred on the true target height are then computed. The purpose of this is to exclude the false tracks during the tracking process.

In the following iteration, the total number of elements (N=7) contained in the aperture are then used in determining the correlation coefficient. This has the advantage of improving the signal-to-noise ratio in the correlation process by a factor which is equal to the square root of the ratio of the number of elements currently being used to that used initially, thereby improving the accuracy of the estimate of the target height. It should be mentioned that once the target track has been identified, the procedure of perturbing the antenna height is of little further use.

In the subsequent iterations of the algorithm, that is, during the process of tracking the target, z_{AV} and z_{INC} are continually updated. In addition, a true estimate of the target height is determined by computing a 2-point running average of the previous estimate of the target height and the present estimate.

In the event that the track is lost due to low signal-to-noise ratios, the tracking process continues for 3 iterations based on the last known estimate of the target height. If, after this period, the target track is not found, then the range of height vectors is expanded to $\pm\Delta z_{AV}$, centered on the last known estimate, and the procedure of perturbing the antenna height is reintroduced so that the true target track can be re-identified.

11.1 RESULTS

The final stage of CHA processing consists of track selection. A demonstration of track-selection is given in Figures 24 to 26 using the same data that was used in Figures 21 to 23. It should be noted that in each instance the algorithm has identified the correct target track and has successfully developed the track over the entire range for which data was available. Bearing in mind that the nominal target heights were respectively 7.39, 5.0 and 10.0 metres, it is readily seen that the tracking accuracy of the algorithm is very high indeed.

12. SUMMARY AND CONCLUSIONS

In this report is given a review of the CHA low-angle tracking technique. In so doing, more analytical results are presented, thereby more clearly demonstrating the basis for the algorithm and documenting the various stages of processing. One stage of the processing that receives considerable attention, because of recent developments, is the track-selection algorithm. This algorithm is based on a perturbation technique, where either the antenna

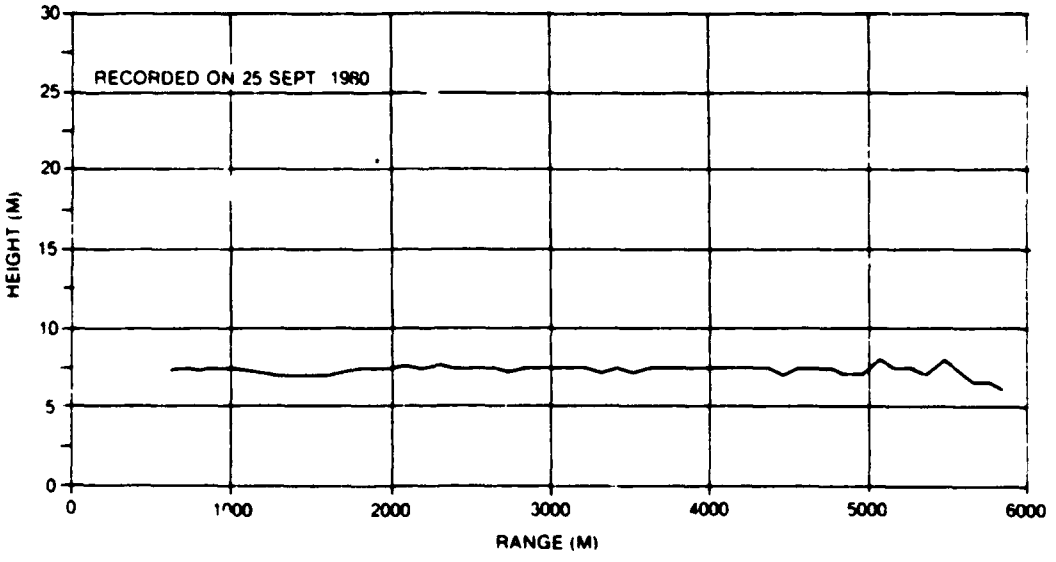

Figure 24. CHA Target Track Obtained From Measured Data; z_2 = 7.39m (Using the Same Data as in Figure 21).

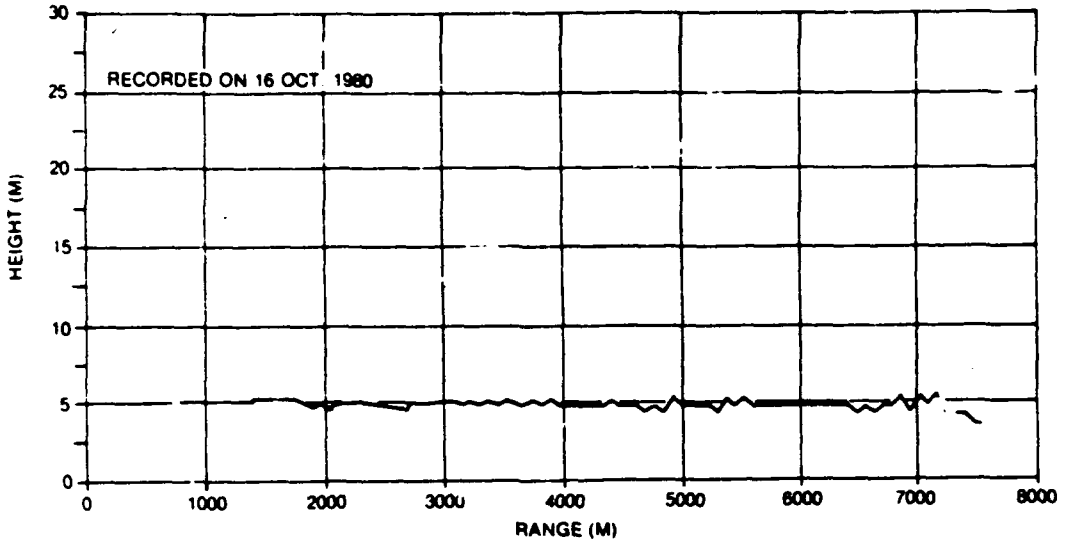

Figure 25. CHA Target Track Obtained From Measured Data; z_2 = 5.0m (Using the Same Data as in Figure 22).

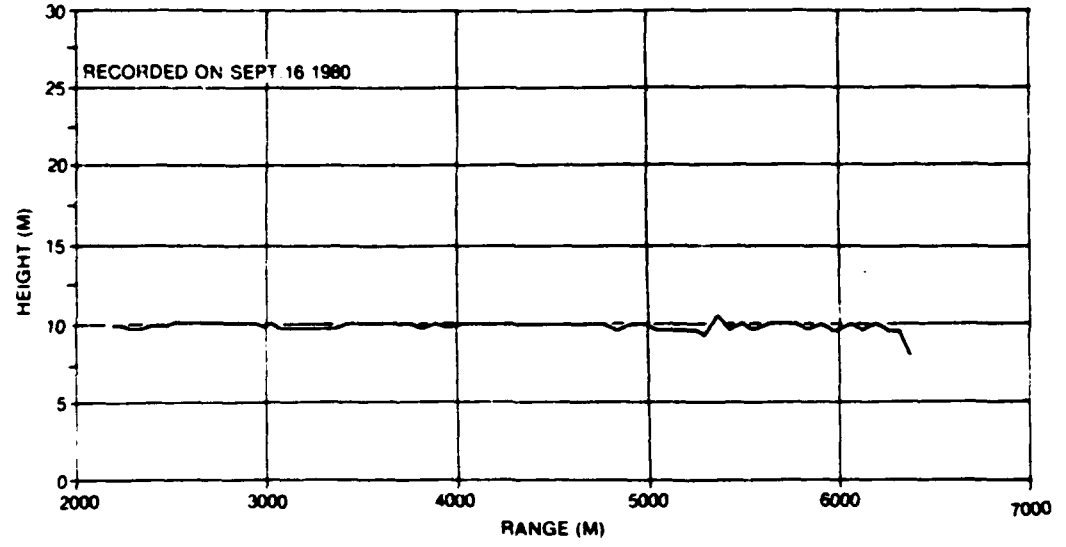

Figure 26. CHA Target Track Obtained From Measured Data; z_2 = 0.0m (Using the Same Data as in Figure 23).

height or RF frequency is purposely varied. It is shown that a change in antenna height of the order of 11% was sufficient to permit successful operation of this algorithm. Basically, this antenna-height variation is sufficiently large to produce deviations on the false tracks which are larger than the deviations on the true track caused by errors in calibration and noise.

A considerable amount of the discussion is centred on the characteristics of the interference pattern at the radar resulting from the direct and indirect rays from the target. This subject was chosen as a topic of discussion so as to set the stage for an introduction to sampled-aperture technology, in particular, the use of a sampled aperture array for recording data which can subsequently be used for testing and developing the CHA algorithm. The algorithm as described here is recast somewhat from that described by Litva[1] so as to be compatible with data recorded with an experimental sampled-aperture radar facility. This report contains a thorough description of the analytical processes inherent to the revised algorithm and its software implementation.

Finally, the algorithm is tested with experimental data recorded over the Ottawa River during the summer of 1980. It is shown that with good calibration of the sampled-aperture facility, the CHA algorithm is capable of tracking low-altitude targets for ranges between 7000 and 500m. In addition, rms tracking accuracies of 2.0m or 0.5 milliradians are demonstrated with target altitudes at least as low as 5.0m.

13. ACKNOWLEDGEMENTS

The authors acknowledge the contributions of Mr. A. Vanderwel, formerly of I.P. Sharp Associates, during the early stages of this project. This work was sponsored by the Department of National Defence, Ottawa, Canada.

14. REFERENCES

1. Litva, J., *A New Low-angle Tracking Technique*, CRC Report No. 1335, May 1980.

2. Freehafer, J.E., W.T. Fishback, W.H. Furry and D.E. Kerr, *Theory of Propagation in a Horizontally Stratified Atmosphere*, Propagation of Short Radio Waves (D.E. Kerr, ed.), McGraw-Hill Book Company, 1951, p. 37.

3. Kerr, D.E., W.T. Fishback and H. Goldstein, *Reflections from the Earth's Surface*, Propagation of Short Radio Waves (D.E. Kerr, ed.), McGraw-Hill Book Company, 1951, p. 396.

4. Fishback, W.T., *Methods for Calculating Field Strength With Standard Refraction*, Propagation of Short Radio Waves (D.E. Kerr, ed.), McGraw-Hill Book Company, 1951, pp. 112-113.

5. Stiefel, E.L., *An Introduction to Numerical Mathematics*, Academic Press, 1966, pp. 83-87.

6. Braun, B.P., *Radar Height Finding*, Radar Handbook (M.I. Skolnik, ed.), McGraw-Hill, 1970, p. 22-10.

7. Kerr, D.E., W.T. Fishback and H. Goldstein, op. cit., p. 406.

8. Beckmann, P. and A. Spizzichino, *The Scattering of EM Waves From Rough Surfaces*, Pergamon Press, 1963.

9. Beard, C.I., *Coherent and Incoherent Scattering of Microwaves From the Ocean*, IEEE Transactions, ANT. PROP., Vol. AP-9, September 1961, pp. 470-483.

10. Nathanson, F.E., *Radar Design Principles*, McGraw-Hill, 1969, Chapter 7.

11. Cold, C. and C.M. Rader, *Digital Processing of Signals*, McGraw-Hill, 1969, Chapter 6.

12. White, W.D., *Double-null Tracking at Low-angles*, First Military Microwave Conference Proc., pp. 127-136, 25-27, October 1978.

13. Monzingo, R.A. and T.W. Miller, *Introduction to Adaptive Arrays*, John Wiley & Sons, 1980.